HHS Public Access

Author manuscript

*Sci Transl Med*. Author manuscript; available in PMC 2019 October 10.

Published in final edited form as:

*Sci Transl Med*. 2019 April 10; 11(487): . doi:10.1126/scitranslmed.aau3259.

# Targeted antibody and cytokine cancer immunotherapies through collagen affinity

**Jun Ishihara**[1,‡], **Ako Ishihara**[1,‡], **Koichi Sasaki**[1], **Steve Seung-Young Lee**[2], **John-Michael Williford**[1], **Mariko Yasui**[3], **Hiroyuki Abe**[3], **Lambert Potin**[1,4], **Peyman Hosseinchi**[1], **Kazuto Fukunaga**[1], **Michal M. Raczy**[1], **Laura T. Gray**[1], **Aslan Mansurov**[1], **Kiyomitsu Katsumata**[5], **Masashi Fukayama**[3], **Stephen J. Kron**[2], **Melody A. Swartz**[1,6], and **Jeffrey A. Hubbell**[1,*]

[1]Institute for Molecular Engineering, University of Chicago, Chicago, IL 60637, USA [2]Department of Molecular Genetics and Cell Biology, The University of Chicago, Chicago, IL 60637, USA [3]Department of Pathology, The University of Tokyo, 113-8655 Tokyo, Japan [4]Institute of Bioengineering, Ecole Polytechnique Fédérale de Lausanne, CH-1015 Lausanne, Switzerland [5]Institute for Molecular Engineering, University of Chicago, Chicago, IL 60637, USA on leave from Astellas Pharma Inc [6]Ben May Department for Cancer Research, University of Chicago, Chicago, IL, 60637, USA

## Abstract

Cancer immunotherapy with immune checkpoint inhibitors (CPI) and interleukin (IL)-2 has demonstrated clinical efficacy but is frequently accompanied with severe adverse events caused by excessive and systemic immune system activation. Here, we addressed this need by targeting both the CPI antibodies anti-cytotoxic T-lymphocyte antigen 4 antibody (αCTLA4) + anti-programmed death-ligand 1 antibody (αPD-L1) and the cytokine IL-2 to tumors via conjugation (for the antibodies) or recombinant fusion (for the cytokine) to a collagen-binding domain (CBD) derived from the blood protein von Willebrand factor (VWF) A3 domain, harnessing the exposure of tumor stroma collagen to blood components due to the leakiness of the tumor vasculature. We show that intravenously (i.v.) administered CBD protein accumulated mainly in tumors. CBD conjugation or fusion decreases the systemic toxicity of both αCTLA4+αPD-L1 combination therapy and IL-2, for example eliminating hepatotoxicity with the CPI molecules and ameliorating pulmonary edema with IL-2. Both CBD-CPI and CBD-IL-2 suppressed tumor growth compared to their unmodified forms in multiple murine cancer models, and both CBD-CPI and CBD-IL-2

*Corresponding author. jhubbell@uchicago.edu.

**Author contributions:** J.I., A.I., M.A.S. and J.A.H. designed the project. J.I., and A.I. performed the experiments. J.I., A.I., and J.A.H. analyzed the data. J.I., A.I., and J.A.H. wrote the paper. K.S., J.M.W., L.P., P.H., K.F., L.T.G., A.M., and K.K. assisted with tumor experiments. M.M.R. assisted with protein mass spectrometry. S.S.L. and S.J.K. assisted with imaging analysis. M.Y., H.A., and M.F. performed the histopathological analysis.

‡These authors contributed equally.

**Competing interests:** J.I., A.I, K.S., K.F., M.A.S. and J.A.H. are inventors on U.S. Provisional Patent applications 62/638,520, 28/984,351, and 62/727,156. J.I., A.I., M.A.S. and J.A.H. are founders and shareholders in Arrow Immune, Inc., which is developing the technology presented in this report, and J.A.H. and M.A.S. have leadership roles in that company. S.S.L. and S.J.K. have founded Transnostics to commercialize tumor imaging methods used here. K.S. is currently affiliated with Kyushu university (Fukuoka, Japan). K.F. is currently affiliated with FUJIFILM Corporation (Kanagawa, Japan). The other authors declare that they have no competing interests.

**Data and materials availability:** All data associated with this study are present in the paper or supplementary materials.

increased tumor-infiltrating $CD8^+$ T cells. In an orthotopic breast tumor model, combination treatment with CPI and IL-2 eradicated tumors in 9 of 13 animals with the CBD-modified drugs, whereas it did so in only 1 of 13 animals with the unmodified drugs. Thus, the A3 domain of VWF can be used to improve safety and efficacy of systemically-administered tumor drugs with high translational promise.

## One Sentence Summary:

An engineered cancer immunotherapy using a collagen-binding domain enhances efficacy and reduces adverse events.

## INTRODUCTION

Immune checkpoint inhibitors (CPI) have demonstrated clinical efficacy in cancer immunotherapy (1, 2). Immune checkpoints are inhibitory pathways used by the immune system to protect cells from excessive immune responses (3). Cytotoxic T-lymphocyte antigen 4 (CTLA4, CD152) is expressed on regulatory T cells (Tregs) and activated T cells (4, 5). In the clinic, anti-CTLA4 antibody (αCTLA4) treatment prolonged survival of melanoma patients (5). Some tumor cells express programmed death-ligand 1 (PD-L1, CD274). Association of PD-L1 with its ligand programmed death 1 (PD-1, CD279) results in inactivation of T cells. Anti-PD-L1 (αPD-L1) blocking antibodies have shown efficacy against several types of cancer (6, 7). Moreover, combination therapy using aPD-1 (nivolumab) and αCTLA4 (ipilimumab) shows prolongation of survival (8) and has been approved by the US Food and Drug Administration (FDA) for treatment of advanced melanoma and renal cell carcinoma. However, CPI treatment also shows severe side effects, including immune-related adverse events (8–10). In combination therapy, 96% of patients experienced adverse events, and 36% of patients discontinued therapy due to adverse events (8).

Interleukin-2 (IL-2: aldesleukin) is a cytokine that induces proliferation and activation of T cells and natural killer (NK) cells (11). Administration of IL-2 has exhibited antitumor effects in the clinic (12), and aldesleukin has been approved by the US FDA for treatment of metastatic melanoma and renal cell carcinoma. In clinical studies, 19% of patients responded to aldesleukin with prolonged survival, but almost all patients experienced treatment-related adverse events, including 1.1% of treatment-related death (13). Aldesleukin has a narrow therapeutic window due to induction of severe adverse events such as pulmonary edema (14).

Because such immunotherapeutics serve to activate immune responses, their side effects are caused by immune activation (10, 15) and typically result from off tumor-target drug action. In a way, patients experiencing adverse events have indeed ‘responded’ to the therapy, as their immune systems have been activated by treatment, but converting these cases into positive clinical outcomes remains an important challenge in the field. One strategy to address this problem is through drug targeting approaches, which seek to deliver drugs only where they are needed, thereby focusing their actions on the disease site. We have previously reported that conjugation of a promiscuous extracellular matrix (ECM)-binding peptide

derived from placenta growth factor-2 (specifically, PlGF-$2_{123–144}$) to CPI antibodies enhanced retention of these antibodies at the peri-tumoral (p.t.) injection site (16). PlGF-$2_{123–144}$ conjugation enhances antitumor efficacy and safety of anti-cytotoxic T-lymphocyte antigen 4 antibody (αCTLA4) + anti-programmed death-ligand 1 antibody (αPD-L1) combination therapy compared to their unmodified forms when injected locally. This approach requires local intra/peri-tumoral injection; although local injection of PlGF-$2_{123–144}$-CPI improved CPI therapy, administration of the drug systemically and having it target to the tumor sites from the blood would improve translational utility and increase the range of applicable cancer types and patients.

Collagen is the most abundant protein in the mammalian body and exists in almost all tissues (17). Collagen, an ECM protein, is richly present in the subendothelial space of the blood vessel as well as the tumor stroma. Because of its insolubility under physiological conditions, collagen barely exists within the blood (18, 19). The vasculature of tumors is hyperpermeable compared to the normal blood vessel, due to an abnormal structure (20). Thus, with this leakiness, collagen in the tumor can be exposed to molecules carried in the bloodstream preferentially to other tissues (21–23). Moreover, many tumor tissues contain increased amounts of collagen compared to normal tissues (24, 25).

von Willebrand factor (VWF), a hemostasis factor, binds to both types I and III collagen (26). When a blood vessel is injured, collagen beneath the endothelial cells is exposed to proteins in the blood, and VWF binding to collagen initiates the thrombosis cascade (26). The VWF A domain has the highest affinity for collagen among reported non-bacterial origin proteins/peptides (27). Particularly within the A domain, the A3 domain of VWF has been reported as a collagen-binding domain (CBD, using this abbreviation to refer specifically to the VWF A3 collagen-binding domain) (28). Here, we hypothesized that CBD conjugation to CPI antibodies and fusion to cytokines such as IL-2 can target these immunotherapeutic molecules to tumors due to the leaky vasculature within the tumor tissue, leading to improved safety and antitumor efficacy by efficient immune system activation within the tumor microenvironment.

## RESULTS

### CBD-conjugated CPI and CBD-fused IL-2 bind to collagens.

We first examined the capacities of CBD-conjugated CPI (CBD-CPI) and CBD-fused IL-2 recombinant protein (CBD-IL-2) to bind collagen in vitro. CPI antibodies were chemically conjugated to human VWF A3 domain recombinant protein (Fig. 1A). Human CBD-fused murine IL-2 was expressed recombinantly. Mass spectrometry analysis and SDS-PAGE revealed that up to 3 CBD protein domains were bound to 1 IgG and exactly 1 CBD protein was fused to 1 IL-2 (fig. S1). Strong binding affinities of CBD-αCTLA4, CBD-αPD-L1, and of CBD-IL-2 against collagen type I and III were observed (Fig. 1B and fig. S2). Importantly, CBD-αCTLA4 and CBD-αPD-L1 recognized their target antigens, and CBD-IL-2 bound to IL-2Ra with similar dissociation constant ($K_D$) values to their unmodified forms (Fig. 1B and fig. S2). CBD-mouse IL-2 and mouse IL-2 similarly induced proliferation of the IL-2-dependent CTLL-2 cell line (fig. S3A). Also, both CBD-human IL-2 and human IL-2 bound to cultured human $CD8^+$ T cells in peripheral blood

mononuclear cells (fig. S3B). These data thus show that CBD-CPI and CBD-IL-2 bind to collagens without impairment of their binding capacities to their targets.

### CBD protein localizes in the tumor after i.v. injection.

We performed an *in vivo* biodistribution analysis to determine if CBD localizes in the tumor microenvironment after i.v. injection through binding to endogenous collagen in orthotopic MMTV-PyMT breast tumor-bearing mice. Fluorescence detection revealed that the CBD protein preferentially localized in the tumor, with lesser localization in the kidney and liver, where the endothelium is fenestrated (Fig. 1C). We then analyzed the localization of the injected CBD-$\alpha$PD-L1 within the tumor (Fig. 1D, E). We observed that i.v. injected CBD-$\alpha$PD-L1, but not unmodified αPD-L1 localized within the stroma, demonstrating greater tumor retention of the CBD-αPD-L1 compared to αPD-L1 (Fig. 1D, E and fig. S4). These data demonstrate tumor targeting of CBD after i.v. injection. Importantly, CBD-IL-2 but not unmodified IL-2 bound around the blood vessels, where collagen I is enriched, within human melanoma sections (Fig. 1F, G).

### CBD-conjugation to CPI and CBD-fusion to IL-2 reduce their side effects.

Because the CBD targeted the tumor, we hypothesized that conjugation or fusion of the CBD to immunotherapeutic drugs would reduce toxicity. The concentrations of both CBD-αCTLA4 and CBD-αPD-L1 in blood serum were lower compared to their unmodified forms (fig. S5A, B). This is presumably due to sequestration of CBD-CPI within the tumor and thus competition of the tumor against the non-diseased tissues. Administration of unmodified CPI (αCTLA4 and αPD-L1 in combination) administration to B16F10-bearing mice increased tumor necrosis factor-a (TNFα) concentrations in serum (indicative of excess activation of the immune system) and induced marked morphological changes and lymphocyte infiltration in the lung and the liver, whereas CBD-CPI did not (Fig. 2A–C and fig. S6A). No statistically significant elevations of lymphocyte infiltration were observed in the kidney in either case (fig. S6B). CPI treatment induced $CD8^+$ T cell but not $CD4^+$ T cell, B cell, or NK cell infiltration into the liver (fig. S7). Unmodified CPI, but not CBD-CPI treatment, increased both alanine aminotransferase (ALT) and aspartate aminotransferase (AST) activity, clinically used liver damage markers, in serum (Fig. 2D, E). An increase of water content in the liver was induced by CPI but not CBD-CPI therapy, suggesting that CBD-CPI therapy maintains the liver structure (Fig. 2F). Injected CBD-IL-2 demonstrated shorter plasma IL-2 pharmacokinetics compared to that of unmodified IL-2 in tumor-bearing mice (fig. S5C). Interestingly, in non-tumor bearing mice, CBD-IL-2 and IL-2 showed similar plasma half-life. Faster clearance of CBD-IL-2 in tumor-bearing mice is presumably due to competition from the tumor for binding. Unmodified IL-2 administration induced splenomegaly and pulmonary edema due to increased vascular permeability (29), whereas CBD-IL-2 did not (Fig. 2G, H). Taken together, these results indicate that CBD conjugation decreases systemic toxicity of both CPI and IL-2 immunotherapy.

### CBD-conjugation to CPI and CBD-fusion to IL-2 improve efficacy in multiple cancer models.

We then examined the antitumor efficacy of CBD-αCTLA4 + CBD-αPD-L1 combination therapy. In B16F10 melanoma, unmodified CPI treatment exhibited small antitumor effects

under this regimen (Fig. 3A). In contrast, CBD-CPI at the same dose as unmodified CPI displayed a further therapeutic effect, slowing tumor growth (Fig. 3A) at both 25 μg and 100 μg single doses of each antibody. Importantly, administration of CPI + CBD protein without conjugation abolished the antitumor effect, indicating that the conjugation of CBD to CPI is indispensable for this action and that free CBD has no intrinsic antitumor activity (fig. S8). We also compared the efficacy of CBD-CPI administered systemically to our earlier published approach on local (p.t.) administration of ECM-binding PlGF-$2_{123–144}$-αCTLA4 and PlGF-$2_{123–144}$-αPD-L1 (16); we observed that systemic targeting of the CBD-CPI molecules achieved similar efficacy as the local administration of the PlGF-$2_{123–144}$-CPI molecules at equal doses (Fig. 3A). In the case of a CT26 colon carcinoma, a single dose of unmodified CPI (combined αCTLA4 and aPD-L1) slowed tumor progression; equidosed CBD-CPI treatment further suppressed tumor growth (Fig. 3B). CBD-CPI also showed higher antitumor efficacy against MMTV-PyMT breast tumors and extended survival of mice compared to unmodified CPI (Fig. 3C, D). Notably, a single dose of CBD-CPI led to complete remission in 6 mice out of 12, and no mice re-challenged with MMTV-PyMT cells developed palpable tumors, whereas all naïve mice grew detectable tumors, demonstrating that CBD-CPI induced immunologic memory (Fig. 3E). CBD-CPI did not show a response against EMT6 breast cancer, which is reportedly an immune excluded tumor, in which there is an antitumor immune response but the immune cells are not able to penetrate into the tumor microenvironment (fig. S9A) (30).

Next, we examined the antitumor efficacy of CBD-IL-2. 6 μg IL-2 or equimolar CBD-IL-2 were injected i.v. in B16F10-bearing mice. At this dose, unmodified IL-2 treatment did not show a clear antitumor effect, consistent with a previous report (31), whereas CBD-IL-2 treatment induced smaller tumor sizes (Fig. 3F). Similarly, CBD-IL-2, but not unmodified IL-2, showed antitumor effects against CT26 and MMTV-PyMT tumors (Fig. 3G–I). CBD-IL-2 slightly delayed EMT6 tumor growth (fig. S9B). This set of data indicates that CBD-IL-2 therapy has superior antitumor effects compared to its unmodified form. Combination therapy of CBD-CPI + CBD-IL-2 administration further suppressed MMTV-PyMT tumor growth and extended survival (Fig. 3J, K). Combined CBD-CPI + CBD-IL-2 administration induced complete remission in 9 out of 13 mice, whereas unmodified control CPI + IL-2 treatment did so in 1 of 13 mice.

### CBD-CPI and CBD-IL-2 enhance antitumor immunity compared to their unmodified forms.

To determine the mechanism behind the therapeutic action of CBD-CPI and CBD-IL-2 treatments, we characterized T cell responses in B16F10 tumor-bearing mice. CBD-CPI increased the frequency of $CD8^+$ T cells of total $CD45^+$ cells within the tumor compared to unmodified CPI and PBS injection (Fig. 4A), whereas the frequency of $CD4^+$ T cells was maintained in all groups (Fig. 4B). CBD-CPI treatment, but not CPI treatment, decreased the percentage of $CD25^+Foxp3^+$ Tregs within the $CD4^+$ T cell population (Fig. 4C). As a consequence, CBD-CPI treatment enhanced effector ($CD62L^-CD44^+$) $CD8^+$ T cell-to-Treg ratios within the tumor, a predictor of therapeutic efficacy (32), compared to equidosed unmodified CPI and PBS treatments (Fig. 4D). To test whether tumor-infiltrating $CD8^+$ T cells produced higher concentrations of effector cytokines, $CD8^+$ T cells were stimulated ex vivo using aCD3 and aCD28. CBD-CPI treatment increased the percentage of $IL2^+$, $TNFα^+$,

and IFN$\gamma^+$ cells in $CD8^+$ tumor-infiltrating T cells compared to the PBS treatment group, whereas unmodified CPI treatment did not (Fig. 4E–G). CBD-CPI reduced the frequency of macrophages and granulocytic myeloid-derived suppressor cells (MDSCs), which are immunosuppressive cells, as well as DCs within the tumor (fig. S10).

As to B16F10 melanoma tumor immune responses to IL-2 treatment, CBD-IL-2 treatment enhanced the number and frequency of tumor-infiltrating $CD8^+$ T cells (Fig. 4H, I). CBD-IL-2 therapy did not increase the expression of the exhaustion marker PD-1 in these $CD8^+$ T cells (fig. S11A). Neither IL-2 nor CBD-IL-2 increased the frequency and number of $CD4^+$ T cells or NK cells within the tumor (Fig. 4J, K and fig. S11B, C). Importantly, CBD-IL-2 increased the frequency of Tregs within $CD4^+$ T cells, to the same extent as IL-2 (fig. S11D–E). CBD-IL-2 increased the number of the Tregs although there was no statistical significant difference. CBD-IL-2 did not increase other immune suppressive cells such as MDSCs nor macrophages within the tumor (fig. S11F–H). The frequency of $CD8^+$ T cells within the spleen was unchanged after CBD-IL-2 therapy (fig. S11I), suggesting tumor-specific $CD8^+$ T cell expansion. CBD-IL-2 did not affect the frequencies of PD-$1^+CD8^+$ T cells within total $CD8^+$ T cells or the frequencies of $CD4^+$ T cells, granulocytic MDSCs, or macrophages in the spleen (fig. S11J–M). CBD-IL-2 slightly increased the frequency of NK cells and slightly decreased the frequency of myelomonocytic MDSCs in the spleen (fig. S11N, O).

In the breast cancer models, CBD-IL-2 but not IL-2 increased the numbers of $CD8^+$ T cells and NK cells within the PyMT tumor but did not change the numbers of $CD4^+$ T cells, the frequencies of PD-$1^+CD8^+$ T cells or Tregs (fig. S12A–E). In contrast, neither CBD-IL-2 nor IL-2 treatment affected the number of $CD8^+$, PD-$1^+CD8^+$, $CD4^+$ T cells, Tregs, or NK cells within the immune excluded EMT6 tumor (fig. S12F–J). Collectively, CBD-CPI and CBD-IL-2 treatment effectively activated tumor-infiltrating T cells, corresponding to the therapeutic effects observed in Fig. 3.

## DISCUSSION

Strategies of targeted tumor therapy can be classified as active targeting or passive targeting (33). Previously, as active targeting strategies, antibodies against proteins that are specifically expressed on tumor cells or in the tumor microenvironment have been developed, including those targeting fibronectin extra domain A, fibroblast activation protein a, carcinoembryonic antigen, and mucin (34–37). Drug conjugates or fusions to these antibodies have shown benefits of tumor targeting. CBD-based tumor targeting is also an active targeting approach, in terms of tumor collagen targeting based on molecular affinity, but it targets a protein that is abundant both throughout the body and in the tumor. CBD-based tumor targeting exploits the pathological structure of tumor vessels, where the vasculature is more permeable than in healthy tissues (38, 39). Thus, the CBD-drugs are tumor microenvironment-specific, yet not by targeting a molecule that is specifically located in the tumor, but rather exploiting tumor-specific accessibility. The CBD may be usable without prior investigation of tumor antigens, because collagen is broadly present in tumors. Moreover, since the CBD does not bind to a tumor cell-specific target, it is not subject to clearance by endocytosis or down-regulation of binding due to mutational loss. As such, the CBD approach turns the tumor stroma matrix into both a drug target and a drug reservoir.

Although the therapeutic effects of CPI and IL-2 in the clinic are remarkable, a number of patients experience serious treatment-related adverse events. In this study, we showed that the incidence of such adverse events caused by CPI and IL-2 therapies was decreased by CBD conjugation or fusion. The reduction of liver and lung toxicity of CPI and reduction of IL-2-induced pulmonary edema induction by CBD association is especially remarkable, because those side effects are commonly observed in patients (10, 14). Although the mechanism of the toxicity of tumor immunotherapeutics may be multifactorial, is complicated and needs detailed future investigation, immunotoxicity in CPI-treated patients is correlated with the concentration of circulating cytokines (40). In our previous study, unmodified CPI showed systemic exposure of injected CPI, up-regulation of circulating cytokine concentrations and liver damage, whereas tumor-localized PlGF-$2_{123–144}$-CPI did not (16). In general, systemic exposure of CPI induces circulating cytokines, which may contribute to tissue damage. CBD conjugation to CPI antibodies and fusion to IL-2 decreased the concentration of the injected drug in the blood by accumulation in the tumor. CBD-CPI did not enhance plasma TNFa concentration, whereas CPI did, which may be one of the mechanisms that contributed to the observed decrease in organ damage. Thus, the decrease in side effects presumably results from competition for the drug by the tumor. Reduction in liver damage was correlated with reduction in $CD8^+$ T cells present in the liver with CBD-CPI treatment compared to unmodified CPI. CBD conjugation to CPI antibody and CBD fusion to IL-2 may even allow decreases in the administered dose, because we observed tumor growth delay at low dosages, where their unmodified forms did not show therapeutic efficacy. These data suggest that CBD-drugs may reduce adverse events associated with immunotherapy.

We have observed enhanced antitumor efficacy of both CBD-CPI and CBD-IL-2 compared to their unmodified forms in multiple tumor models. These data suggest that the approach of collagen targeting by the VWF A3 domain is generally applicable to multiple types of solid tumors. EMT6 tumors were less responsive to the CBD-CPI and CBD-IL-2 therapies, suggesting that immune cell recruitment to this immune-excluded tumor is necessary to achieve favorable response to therapy with these pathways.

Notably, we observed that systemic injection of CBD-CPI showed similar antitumor efficacy as the local (p.t.) administration of PlGF-$2_{123–144}$-CPI therapy, which is then retained in the tumor injection site through matrix affinity (16). CBD-CPI therapy demonstrated clear antitumor immune system activation within the tumor (for example, increased numbers of $CD8^+$ T cells and stimuli-responsive $CD8^+$ T cells), presumably due to increases in the amount of CPI antibody within the tumor, as we observed with CBD-αPD-L1 by imaging analysis. In this study, we tested CBD-αPD-L1, but the use of CBD-αPD-1 may show similar antitumor effects, as the antitumor effect of αPD-L1 and aPD-1 are similar (41). CBD-CPI treatment, but not unmodified CPI treatment, decreased the percentage of Tregs within the $CD4^+$ T cell population, supporting the tumor-targeting ability of CBD-αCTLA4, because we used αCTLA4 with Treg depletion capacity (42).

IL-2 shows an antitumor effect through inducing proliferation of $CD8^+$ T cells. Thus, with tumor targeting, our data show that CBD-IL-2 increased the numbers of tumor-infiltrating $CD8^+$ T cells compared to unmodified IL-2. We also observed an expansion of intratumoral

Tregs in some tumor types. Because CBD-IL-2 binds to IL-2Rα (CD25) with a similar affinity to IL-2, we assume that CBD-IL-2 acts on both $CD8^+$ T cells and Tregs. Previous reports using Fc-fused IL-2 observed both $CD8^+$ T cell and Treg expansion within B16F10 tumor, concluding that Treg expansion did not affect efficacy of the therapy dramatically (31). The increased number of $CD8^+$ T cells may be enough to have some antitumor efficacy with the IL-2 therapy, even if Treg number is increased at the same time. Thus, we believe that expansion of $CD8^+$ T cells mainly contribute to the antitumor efficacy of CBD-IL-2.

Because tumor antigen-specific T cells are enriched around tumors (43, 44), CBD-CPI and CBD-IL-2 may effectively activate and expand these T cells, providing superior antitumor efficacy compared to their unmodified forms. CBD-CPI and CBD-IL-2 therapies showed less favorable antitumor effects on the immune-excluded tumor model EMT6, supporting this hypothesis.

The main translational advantage of our approach for tumor-targeted immunotherapy is the systemic delivery route; tumor targeting through CBD association resulted in improvements of both safety and efficacy. Importantly, CBD-IL-2 can bind to human melanoma sections, consistent with the presence of collagen in the human tumor microenvironment (30). For clinical translation of CBD-drugs, an advantage lies in the use of a CBD protein that naturally exists in the blood, here the A3 domain from VWF, limiting the possibility of immune system recognition. Also, the CBD protein can be conjugated to CPI antibodies with a simple chemical reaction. The advantage of this feature is in simplicity of production, in that it is possible to work with antibodies for which production has already been optimized. The CBD conjugation synthesis reaction for antibodies can be done in only 90 minutes, using chemistry that is analogous to PEGylation of proteins. This same reaction is used in antibody-drug conjugates, such as in the production of trastuzumab emtansine (45). As to CBD-IL-2, given that cytokines are smaller and are generally easy to produce, we chose to recombinantly fuse rather than conjugate the CBD to IL-2. These features may facilitate development of CBD-immunotherapy drugs to overcome the barriers to clinical translation.

One limitation of the CBD-based tumor targeting approach is that it is only relevant for solid tumors. Moreover, targeting depends on vascular permeability, which may be different in different tumors. For example, it may be difficult to reach tumors that have poor vasculature or limited angiogenesis. Also, CBD-drugs may potentially localize in unfavorable sites, such as wounds, where collagen is exposed to components of the bloodstream.

In conclusion, we have developed CBD-conjugated/fused cancer immunotherapy drugs, showing the concept with two structurally different molecular classes, two antibodies and a cytokine. We found that CBD association enhanced antitumor activity and reduced adverse effects of both αCTLA4 and αPD-L1 combination therapy and IL-2. Our approach demonstrates an interesting methodology (high affinity protein domains derived from a protein that naturally exists in the blood) and biological approach (targeting a protein that is abundant in the body but that is only exposed in the tumor via its leaky vasculature). This simple approach of an engineered collagen-binding immunotherapy may hold potential for clinical translation as a tumor-targeted immunotherapeutic.

# MATERIALS AND METHODS

## Study design

This study was designed to test the strategy of targeting immunotherapeutics to tumors through engineered affinity for collagen. Specifically, we tested whether antitumor efficacy and adverse effects of CBD-CPI and CBD-IL-2 against mouse models of melanoma, colon carcinoma and breast cancer are improved compared to their unmodified forms. We measured tumor growth, the antitumor immune response, and various aspects of toxicity after treatment. These experiments were designed to develop therapeutic strategies to improve the conventional forms of CPI and IL-2 in the clinic. Statistical methods were not used to predetermine necessary sample size, but sample sizes were chosen based on estimates from pilot experiments and previously published results such that appropriate statistical tests could yield significant results. Production of CBD-CPI and CBD-IL-2 was performed by multiple individuals to ensure reproducibility. All experiments were replicated at least twice except for fig S4, S5, S7, S10, S11(F-O), and S12 (once). For animal studies, mice were randomized into treatment groups within a cage immediately before the first drug injection and treated in the same way. Samples were excluded from analysis only when an animal developed a health problem for a non-treatment-related reason, according to the animal care guidelines. The survival endpoint was reached when the tumor size exceeded 500 $mm^3$. The n values used to calculate statistics are indicated in the figure legends. Drug administration and pathological analyses were performed in a blinded fashion. Statistical methods are described in the “Statistical analysis” section. Original data are located in Data file S1.

## Production and purification of recombinant VWF A3 domain and IL-2 protein

The sequences encoding the human VWF A3 domain residues Cys1670-Gly1874 (907–1111 of mature VWF), mouse IL-2, human IL-2, and the fusion of human VWF A3 domain, a $(GGGS)_2$ linker, and mouse IL-2 were synthesized and subcloned into the mammalian expression vector pcDNA3.1(+) by Genscript. A sequence encoding 6 His was added at the N-terminus for further purification of the recombinant protein. Suspension-adapted HEK-293F cells were routinely maintained in serum-free FreeStyle 293 Expression Medium (Gibco). On the day of transfection, cells were inoculated into fresh medium at a density of $1 \times 10^6$ cells/mL. 2 μg/mL plasmid DNA, 2 μg/ml linear 25 kDa polyethylenimine (Polysciences), and OptiPRO SFM medium (4% final concentration, Thermo Fisher) were sequentially added. The culture flask was agitated by orbital shaking at 135 rpm at 37°C in the presence of 5% $CO_2$. 6 days after transfection, the cell culture medium was collected by centrifugation and filtered through a 0.22 μm filter. Culture medium was loaded into a HisTrap HP 5 mL column (GE Healthcare), using an ÄKTA pure 25 (GE Healthcare). After washing the column with wash buffer (20 mM imidazole, 20 mM $NaH_2PO_4$, 0.5 M NaCl, pH 7.4), protein was eluted with a gradient of 500 mM imidazole (in 20 mM $NaH_2PO_4$, 0.5 M NaCl, pH 7.4). The eluate was further purified with size exclusion chromatography using a HiLoad Superdex 200PG column (GE Healthcare). All purification steps were carried out at 4°C. The expression of VWF A3 domain was determined by western blotting using anti-His tag antibody (BioLegend), and the proteins were verified as >90% pure by SDS-PAGE. Amino acid sequences of produced proteins are shown in supplementary table S1.

### Synthesis of CBD-CPI antibody

The synthesis was performed as described previously for PlGF-$2_{123–144}$ conjugates (16). Rat anti-mouse PD-L1 (clone: 10F.9G2, Bio X Cell) and hamster anti-mouse CTLA4 (clone: 9H10, Bio X Cell) were incubated with 15 eq. of sulfo-SMCC for 40 min at room temperature (RT). Excess sulfo-SMCC was removed using a Zeba spin desalting column (Thermo Fisher Scientific). >10 eq. of CBD protein (the VWF A3 domain, with an C-terminal cysteine residue) was then added and reacted for 1 hour at RT.

## MALDI-TOF MS

Antibody solutions were purified by size exclusion column chromatograph as described above to exchange the buffer to PBS. Antibodies were analyzed by MALDI-TOF MS (Bruker Ultraflextreme MALDI TOF/TOF). All spectra were collected with acquisition software Bruker flexControl and processed with analysis software Bruker flexAnalysis. First, a saturated solution of the matrix, α-cyano-4-hydroxycinnamic acid (Sigma-Aldrich), was prepared in 50:50 acetonitrile:1% TFA in water as a solvent. The analyte in PBS (5 μL, 0.1 mg/mL) and the matrix solution (25 μL) were then mixed, and 1 μL of that mixture was deposited on the MTP 384 ground steel target plate. The drop was allowed to dry in a nitrogen gas flow, which resulted in the formation of uniform sample/matrix co-precipitate. All samples were analyzed using high mass linear positive mode method with 2500 laser shots at the laser intensity of 75%. The measurements were externally calibrated at three points with a mix of carbonic anhydrase, phosphorylase B, and bovine serum albumin.

### Sodium dodecyl sulfate polyacrylamide gel electrophoresis (SDS-PAGE)

SDS-PAGE was performed as described previously for PlGF-$2_{123–144}$ conjugates (16, 46). SDS-PAGE was performed on 4–20% gradient gels (Bio-Rad) after IL-2 was reduced with 10 mM DTT. After electrophoresis, gels were stained with SimplyBlue SafeStain (Thermo Fisher Scientific) according to the manufacturer's instruction. Gel images were acquired with the ChemiDoc XRS+ system (Bio-Rad).

### Detection of CPI antibody binding to collagen and their target proteins

The affinity measurement was performed as described previously for PlGF-$2_{123–144}$ conjugates (16, 46). 96-well ELISA plates (Greiner Bio One) were coated with 10 μg/mL collagen I (EMD Millipore), collagen III (EMD Millipore), recombinant mouse (rm)CTLA4 (Sino Biological), or rmPD-L1 (Sino Biological) in PBS for 1 hour at 37°C, followed by blocking with 2% BSA in PBS with 0.05% Tween 20 (PBS-T) for 1 hour at RT. Then, wells were washed with PBS-T and further incubated with 10 μg/mL CBD- or unmodified CPI for 1 hour at RT. After 3 washes with PBS-T, wells were incubated for 1 hour at RT with horseradish peroxide (HRP)-conjugated antibody against rat IgG or Syrian hamster IgG (Jackson ImmunoResearch). After washes, bound CPI antibodies were detected with tetramethylbenzidine substrate by measurement of the absorbance at 450 nm with subtraction of the measurement at 570 nm. The apparent dissociation constant ($K_D$) values were obtained by nonlinear regression analysis in Prism software (v7, GraphPad Software) assuming one-site specific binding.

### Detection of CBD-IL-2 binding to collagen proteins and its receptor

The affinity measurement was performed as described previously for PlGF-$2_{123–144}$ conjugates (16, 46). 96-well ELISA plates were coated with 10 μg/mL collagen I (EMD Millipore), collagen III (EMD Millipore), or 1 μg/mL recombinant mouse IL-2Ra (SinoBiological) in PBS for 1 hour at 37°C, followed by blocking with 2% BSA in PBS-T for 1 hour at RT. Then, wells were washed with PBS-T and further incubated with 10 μg/mL CBD- or unmodified IL-2 for 1 hour at RT. After 3 washes with PBS-T, wells were incubated for 1 hour at RT with biotinylated antibody against IL-2 (eBioscience) and then incubated with HRP-conjugated streptavidin (eBioscience) for 1 hour at RT. After washes, bound CBD-IL-2 and IL-2 were detected with tetramethylbenzidine substrate by measurement of the absorbance at 450 nm with subtraction of 570 nm. The apparent $K_D$ values were obtained by nonlinear regression analysis in Prism software (v7, GraphPad Software) assuming one-site specific binding.

### Proliferation assay

CTLL-2 cells (American Type Culture Collection, ATCC) were cultured in RPMI 1640 (ATCC), supplemented with 10% heat-inactivated fetal bovine serum (FBS), 2 mM L-glutamine, 1 mM sodium pyruvate, 100 U/mL penicillin-streptomycin, and 10 ng/mL recombinant mouse IL-2 (Peprotech). Cells were passaged twice a week to a density of 10,000 cells/mL. For proliferation assays, cells were seeded in a 96-well U-bottom cell culture plate at 10,000 cells/well, and mouse IL-2 and CBD-IL-2 were added at indicated concentrations. The concentration of CBD-IL-2 is presented on an IL-2 basis (for example, 1 ng/mL on IL-2 basis, equivalent to 2 ng/mL CBD-IL-2), in a final volume of 100 μL. Cells were cultured for 48 hours. Cell proliferation was analyzed using CyQUANT Cell Proliferation Assay Kit (Invitrogen) according to the manufacturer's instructions. Fluorescence was measured using a BioTek Cytation 3 Cell Imaging Multi-Mode Reader (Thermo Fisher). A dose response curve was fit via nonlinear regression using GraphPad Prism 7 software (GraphPad).

### Human IL-2 binding to PBMC

Human IL-2 and CBD-human IL-2 were expressed and purified as described above, followed by DyLight 488 (Thermo Fisher) conjugation, and unreacted dye was removed by a Zebaspin spin column (Thermo Fisher) according to the manufacturer's instruction. Protein concentration was determined using a BCA assay kit (Thermo Fisher). PBMCs were purchased from STEMCELL TECHNOLOGY. $5\times10^5$ cells/well were seeded in a 96-well microplate. After culturing in RPMI 1640 containing 10% FBS for 2 days, cells were incubated with 1 μg/mL DyLight 488-labeled IL-2 or equimolar DyLight 488-labeled CBD-IL-2, anti-human CD8, anti-human CD3, and anti-human CD45 antibodies for 60 min on ice. Cells were analyzed by flow cytometry as described below. Obtained mean fluorescence intensity was normalized to the molecular size, considering that CBD-IL-2 showed twice higher fluorescence intensity compared to that of IL-2.

### Mice and cell lines

The mice and cell lines were as described previously (16, 46). C57BL/6 and Balb/c mice, age 8 to 15 weeks, were obtained from the Jackson Laboratories. FVB mice, age 8 to 12 weeks, were obtained from the Charles River. Experiments were performed with approval from the Institutional Animal Care and Use Committee of the University of Chicago. B16F10 cells, CT26 cells and EMT6 cells were obtained from ATCC and cultured according to the instructions. MMTV-PyMT cells were obtained from spontaneously developed breast cancer in FVB-Tg (MMTV-PyVT) transgenic mice (polyoma middle T antigen oncogene expression was induced by mouse mammary tumor virus promotor) and cultured. All cell lines were checked for mycoplasma contamination by a pathogen test IMPACT I (IDEXX BioResearch).

### In vivo biodistribution study

The VWF A3 domain protein was fluorescently labeled using DyLight 800 NHS ester (Thermo Fisher), and unreacted dye was removed by a Zebaspin spin column (Thermo Fisher) according to the manufacturer's instruction. A total of $5 \times 10^5$ MMTV-PyMT cells re-suspended in 50 μL of PBS were injected subcutaneously into the mammary fat pad on the right side of each FVB mouse. When the tumor reached 500 $mm^3$, 300 μg of DyLight 800 labeled CBD or equal amount of DyLight 800 dye was injected i.v.. 48 hours after injection, mice were sacrificed and were perfused transcardially with 10 mL PBS. Organs (heart, lung, stomach, tumor, kidney, spleen, and liver) were extracted and imaged with the Xenogen IVIS Imaging System 100 (Xenogen) under the following conditions: f/stop: 2; optical filter excitation 745 nm; emission 800 nm; exposure time: 1 sec; small binning. Signals of the VWF A3 domain (CBD) proteins were obtained by subtracting signals of DyLight 800 dye from signals of DyLight 800-CBD protein in each organ. % of distribution of CBD protein in each organ was determined by signals of CBD protein in each organ/total signals of CBD protein×100.

### Histological analysis of injected CBD-αPD-L1 within tumor

αPD-L1 (BioXcell, clone 10F.9G2) and αCD31 (BioLegend, clone MEC13.3) were purchased. CBD-αPD-L1 was synthesized and purified as described above. The antibodies were conjugated to NHS-DyLight 594 or 633 fluorescent dyes (Thermo Fisher) at antibody/dye molecule molar ratio of 1:30. Reactions were incubated with gentle agitation at 4°C overnight, followed by dialysis in 10 kDa MWCO Slide-A-Lyzer cassettes (Thermo Fisher) against PBS pH 7.4 at 4°C for 3 days. Fluorescent antibody solutions were stored at 4°C. DyLight594-αPD-L1 (100 μg) or DyLight594-CBD-αPD-L1 (100 μg) was intravenously injected into MMTV-PyMT tumor-bearing mice. 30 min after injection (when the majority of αPD-L1 was not internalized into cells), tumors were harvested and prepared for microscopy as previously described (47). In brief, tumor tissues were washed with cold PBS, fixed with 2% paraformaldehyde in PBS for 10 min at RT, and washed with PBS. Then, tumors were cast in 2% agarose gel (dissolved in distilled water, LE Quick Dissolve Agarose, GeneMate) in 24-well plates. The gel plugs containing tumors were mounted on a vibrating microtome (VT1200S, Leica) equipped with a buffer tray. Sections (at 0.4 mm thickness) were collected in cold PBS. The macrosections were stained with DyLight633-

αCD31 in staining buffer (SB, RPMI 1640 medium with 10 mg/mL BSA and 0.1 % Triton X-100) at 4°C overnight. The macrosections were incubated sequentially in 10 mL of 20, 50, and 80 (w/v) % D-fructose solution for 30 min, 30 min, and 1 hour, respectively, at 25°C with gentle agitation in 20 mL glass vials. A Leica TCS SP8 confocal laser scanning microscope, a white light laser, and a Leica HCX PL APO 10X/0.4 NA dry objective (2.2 mm working distance) were used for imaging with 594 nm excitation and 600–620 nm filters for DyLight594, and 633 nm excitation and 637–655 nm filters for DyLight633. All image analysis was conducted with basic functions in Fiji software. We visually determined the cutoff threshold for the antibodies and CD31 channel images and converted into binary (8 bit) images. The tumor area was determined by outlining tumor boundary in the image data. To measure the distance of antibody from $CD31^+$ tumor vasculature, we applied a distance map to the tumor blood vessel images.

### CBD-IL-2 binding to human melanoma tissue

Human melanoma frozen tissue sections were purchased from OriGene Technologies. The tissues were blocked with 2% BSA in PBS-T for 1 hour at room temperature. Tissue was incubated with 25 μg/mL of mouse IL-2 or equimolar CBD-mouse IL-2 in PBS-T for 2 hours at room temperature. The tissues were stained with hamster anti-human CD31 antibody (Abcam), goat anti-mouse IL-2 antibody (R and D systems), and rabbit anti-collagen I antibody (Abcam) for 1 hour at room temperature. After staining with the fluorescently tagged secondary antibodies, slides were covered with ProLong gold antifade mountant with DAPI (Thermo fisher scientific). An IX83 microscope (Olympus) was used for imaging. Images were processed using ImageJ software (NIH).

### Blood concentration analysis of injected CPI and IL-2

The blood concentration analysis for CPI was performed as described previously (16). $5 \times 10^5$ B16F10 melanoma cells were injected intradermally on the left side of the back of each mouse. IL-2 and CBD-IL-2 were fluorescently tagged using Dylight 800 NHS (Thermo Fisher) according to the manufacturer's instruction. After 4 days, mice were injected with 100 μg each of CPI i.v.. Blood samples were collected in protein low-binding tubes (Eppendorf) on 1, 2, 4, and 6 days after CPI injection, followed by > 4 hour incubation at 4°C. After 7 days, 21 μg of IL-2 or CBD-IL-2 (30 μg on IL-2 basis, equivalent to 60 μg CBD-IL-2) were injected i.v.. For IL-2, blood samples were collected in EDTA-containing heparinized tubes 1 and 10 min after IL-2 injection. Concentrations of CPI in serum were measured by ELISA as described above. Concentrations of IL-2 in plasma were measured with a LI-COR Infrared Odyssey Imager. Plasma half-life was estimated by a simple linear regression model using Prism software (v7, GraphPad).

### Serum cytokine concentration analysis

The serum cytokine concentration analysis was performed as described previously (16). $5 \times 10^5$ B16F10 melanoma cells were injected intradermally on the left side of the back of each 15-week-old C57BL/6 mouse. After 4 and 7 days, mice received two doses of CBD- or unmodified CPI (αPD-L1 and αCTLA4, 100 μg each) i.v.. Blood samples were collected in protein-low binding tubes (Eppendorf) on day 8, followed by overnight incubation at 4°C.

Cytokine concentrations in serum were measured by Ready-SET-Go! ELISA kits (eBioscience) according to the manufacturer's protocol.

### ALT and AST activity analysis

The liver damage marker analysis was performed as described previously (16, 46). B16F10 tumor-bearing mice received CPI injection (αPD-L1 and αCTLA4, 100 μg each), 4 and 7 days after tumor inoculation. On day 10, blood samples were collected in tubes, followed by > 4 hour incubation at 4°C. On the same day, serum was collected and ALT and AST activities were measured by an ALT assay kit or an AST assay kit (both Sigma-Aldrich) according to the manufacturer's protocol.

### CPI treatment effect on liver water content

B16F10 tumor-bearing mice received CPI injection (αPD-L1 and αCTLA4, 100 μg each), 4 and 7 days after tumor inoculation. On day 10, liver was harvested and weighed. Water content in the liver was determined by weighing before and after overnight lyophilization using FreeZone 6 Benchtop Freeze Dryer (Labconco).

### Liver lymphocyte analysis after CPI treatment

B16F10 tumor-bearing mice received CPI injection (αPD-L1 and αCTLA4, 100 μg each), 4 and 7 days after tumor inoculation. On day 10, the liver was harvested and digested, followed by flow cytometric analysis described below.

### Liver, lung and kidney histology

The histological analysis was performed as described previously (16, 46). B16F10 tumor-bearing mice received CBD- or unmodified CPI injection (αPD-L1 and αCTLA4, 100 μg each), 4 and 7 days after tumor inoculation. 10 days after tumor inoculation, mice were euthanized with $CO_2$ inhalation. Then, liver, lung, and kidney were collected and fixed with 2% paraformaldehyde. After embedding in paraffin, blocks were cut into 5 μm sections, followed by staining with hematoxylin and eosin. Images were captured with an EVOS FL Auto microscope (Life Technologies). For quantification of lymphocytic infiltration, the number of lymphocyte infiltration foci in 10 high-power fields (x400) was counted with light microscopy (BX53, Olympus). Slides were evaluated independently by two pathologists (H.A. and M.Y.) who were blinded to the treatment grouping. Microscopic images were captured with color CCD camera (DP27, Olympus).

### The IL-2 treatment effect on lung and spleen

A total of $5 \times 10^5$ B16F10 cells re-suspended in 50 μL of PBS were inoculated intradermally on the left side of the back of each C57BL/6 mouse on day 0. IL-2 (6 μg), or CBD-IL-2 (6 μg on IL-2 basis, equivalent to 12 μg of CBD-IL-2) was injected i.v. on day 7, 8, and 9. On day 10, spleen and lung were harvested and weighed. Water content in the lung was determined by weighing before and after overnight lyophilization using FreeZone 6 Benchtop Freeze Dryer (Labconco).

### Antitumor efficacy of CPI and IL-2 on B16F10 tumor

The measurement of antitumor efficacy was performed as described previously for PlGF-$2_{123–144}$ conjugates (16, 46). A total of $5 \times 10^5$ B16F10 cells re-suspended in 50 μL of PBS were inoculated intradermally on the left side of the back of each C57BL/6 mouse. After 4 days, mice were injected with CBD- or unmodified CPI (αPD-L1 and αCTLA4, 25 μg or 100 μg each), IL-2 (6 μg), or CBD-IL-2 (6 μg on IL-2 basis, equivalent to 12 μg of CBD-IL-2). PlGF-$2_{123–144}$ conjugated CPI (αPD-L1 and αCTLA4, 100 μg each) was prepared and injected peri-tumorally as described previously (16). Tumors were measured with a digital caliper starting 4 days after tumor inoculation, and volumes were calculated as ellipsoids, where V = 4/3 × 3.14 × depth/2 × width/2 × height/2. Mice were sacrificed at the point when tumor volume had reached over 500 $mm^3$.

### Antitumor efficacy of CPI and IL-2 on CT26 tumor

The measurement of antitumor efficacy was performed as described previously for PlGF-$2_{123–144}$ conjugates (46). A total of $5 \times 10^5$ CT26 cells re-suspended in 50 μL of PBS were inoculated intradermally on the left side of the back of each Balb/c mouse. After 5 days, mice were injected i.v. with CBD- or unmodified CPI (αPD-L1 and αCTLA4, 25 μg or 100 μg each), IL-2 (6 μg), or CBD-IL-2 (6 μg on IL-2 basis, equivalent to 12 μg of CBD-IL-2). Tumors were measured with a digital caliper starting 5 days after tumor inoculation as described above. Mice were sacrificed at the point when tumor volume had reached over 500 $mm^3$.

### Antitumor efficacy of CPI, IL-2, and CPI + IL-2 combination on MMTV-PyMT tumor

The measurement of antitumor efficacy was performed as described previously for PlGF-$2_{123–144}$ conjugates (16, 46). A total of $5 \times 10^5$ MMTV-PyMT cells re-suspended in 50 μL of PBS were injected subcutaneously into the mammary gland on the right side of each FVB mouse. After 7 days, mice were injected i.v. with CPI (αPD-L1 and αCTLA4, 100 μg each), IL-2 (6 μg), or CBD-IL-2 (6 μg on IL-2 basis, equivalent to 12 μg CBD-IL-2). For combination therapy of CPI and IL-2, CPI (αPD-L1 and αCTLA4, 25 μg each) and 6 μg IL-2 were administrated on days 7, 14, and 21. Tumors were measured with a digital caliper as described above. Mice were sacrificed when tumor volume reached over 500 $mm^3$. For tumor re-challenge, 30 days after the first tumor inoculation in the right mammary gland fat pad, $5 \times 10^5$ MMTV-PyMT cells were inoculated into the left mammary gland fat pad in CBD-CPI treated tumor-free survivors or in naïve mice.

### Antitumor efficacy of CPI and IL-2 on EMT6 tumor

A total of $5 \times 10^5$ EMT6 cells re-suspended in 50 μL of PBS were inoculated subcutaneously into the mammary gland on the right side of each Balb/c mouse. Mice were injected i.v. with CBD- or unmodified CPI (αPD-L1 and αCTLA4, 100 μg each) on days 7 and 10. IL-2 (6 μg), or CBD-IL-2 (6 μg on IL-2 basis, equivalent to 12 μg CBD-IL-2) were injected on days 7, 10, and 13. Tumors were measured with a digital caliper starting 7 days after tumor inoculation as described above. Mice were sacrificed at the point when tumor volume had reached over 500 $mm^3$.

### Tissue and cell preparation and immune cell subset analysis

The immune cell subset analysis was performed as described previously (16). $5 \times 10^5$ B16F10 melanoma cells were injected intradermally on the left side of the back of each C57BL/6 mouse. A total of $1 \times 10^6$ MMTV-PyMT cells or $5 \times 10^5$ EMT6 cells were inoculated subcutaneously into the mammary gland on the right side of each FVB mouse or Balb/c mouse, respectively. Mice were injected i.v. with CPI (αPD-L1 and αCTLA4, 100 μg each) on day 4, or with 6 μg of IL-2 on days 7, 8, and 9 (B16F10) on two consecutive days after tumor size reached 50 $mm^3$ (MMTV-PyMT), or on days 7 and 8 (EMT6). B16F10-bearing mice were sacrificed on day 8 (CPI T/NK cell analysis), 10 (CPI MDSC analysis) or 10 (IL-2). MMTV-PyMT-bearing mice were sacrificed one day after the second injection. EMT6-bearing mice were sacrificed on day 9. Tumors, livers and spleens were harvested and were digested in Dulbecco's Modified Eagle Medium (DMEM) supplemented with 2% FBS, 2 mg/mL collagenase D, and 40 μg/mL DNase I (Roche) for 30 min at 37°C. Single-cell suspensions were obtained by gently disrupting the liver, spleen, and enzyme-treated tumor through a 70-μm cell strainer. Red blood cells were lysed with ACK lysing buffer (Quality Biological). Cells were counted and re-suspended in Iscove's Modified Dulbecco's Medium (IMDM) supplemented with 10% FBS and 1% penicillin/streptomycin (full medium; all from Life Technologies) and used for flow cytometry staining.

### Ex vivo T cell stimulation

The ex vivo T cell stimulation was performed as described previously (16). Single cell suspensions from tumor were prepared as described above. $CD8^+$ T cells were isolated using EasySep kits (STEMCELL Technologies) following the manufacturer's instructions, except that biotinylated aCD105 (12403, BioLegend) was added to the EasySep $CD8^+$ T cell Isolation Cocktail to remove B16F10 melanoma cells. 96-well cell culture plates (BD Falcon) were coated with 10 μg/mL aCD3 (145–2C11, BioLegend) in PBS overnight at 37°C. Extracted T cells from tumors were plated in 96-well plates and cultured in full medium for 6 hours at 37°C in the presence of 2 μg/mL aCD28 (EL-4, BioLegend) and 5 μg/mL brefeldin A (Sigma-Aldrich). Cells were harvested, stained, and analyzed by flow cytometry as described below.

### Flow cytometry and antibodies

The flow cytometric analysis was performed as described previously (16). Single cell suspensions from tissues were prepared as described above. Antibodies against the following molecules were used throughout the paper if not otherwise indicated: anti-mouse CD3 (145–2C11, BD Biosciences), anti-human CD3 (UCHT1, BD Pharmingen), CD4 (RM4–5, BD Biosciences), anti-mouse CD8α (53–6.7, BD Biosciences), anti-human CD8α (SK1, BioLegend), CD25 (PC61, BD Biosciences), anti-mouse CD45 (30-F11, BD Biosciences), anti-human CD45 (2D1, eBioscience), CD44 (IM7, BD Biosciences), CD62L (MEL-14, BD Biosciences), PD-1 (29F.1A12, BD Biosciences), NK1.1 (PK136, BD Biosciences), Foxp3 (MF23, BD Biosciences), F4/80 (T45–2342, BD Biosciences), MHCII (M5/114.15.2, BioLegend), Ly6G (1A8, BioLegend), Ly6C (HK1.4, BioLegend), CD11b (M1/70, BioLegend), CD11c (HL3, BD Biosciences), B220 (RA3–6B2, BioLegend), IL-2 (JES6–5H4, BD Biosciences), IFNγ (XMG1.2, BD Biosciences), and TNFα (MP6-XT22,

eBioscience). Fixable live/dead cell discrimination was performed using Fixable Viability Dye eFluor 455 (eBioscience) according to the manufacturer's instructions. Staining was carried out on ice for 20 min if not indicated otherwise, and intracellular staining was performed using the Foxp3-staining kit according to manufacturer's instructions (BioLegend). After a washing step, cells were stained with specific antibodies for 20 min on ice before fixation. All flow cytometric analyses were done using a Fortessa (BD Biosciences) flow cytometer and analyzed using FlowJo software (Tree Star).

### Statistical analysis

The statistical significance of differences between experimental groups was assessed using Prism software (v7, GraphPad). Where one-way ANOVA followed by Tukey's HSD post hoc test was used, variance between groups was found to be similar by Brown-Forsythe test. For non-parametric data, Kruskal-Wallis test followed by Dunn's multiple comparison test was used. For single comparisons, a two-tailed Student's *t*-test was used. Survival curves were analyzed using the log-rank (Mantel–Cox) test. The symbols * and ** indicate P values less than 0.05 and 0.01, respectively; N.S., not significant.

## Supplementary Material

Refer to Web version on PubMed Central for supplementary material.

## Acknowledgements:

We thank the Human Tissue Resource Center of the University of Chicago for histology analysis. We thank A. Solanki for assistance in tail vein injections and S. Gomes for experimental help.

**Funding:** This work was supported by the European Research Commission grant Cytrix (J.A.H.). This work was supported in part by National Cancer Institute R01 CA199663 (S.J.K.) and by National Institute of Biomedical Imaging and Bioengineering K99 EB022636 (S.S.L.). K.S. is supported by Research Fellowship for Young Scientists (JSPS, JP17J05032) and Advanced Graduate Course on Molecular Systems for Devices (Kyushu University). L.P. is funded by the Fonds Pierre-François Vittone.

## REFERENCES

1. Allison JP, Immune checkpoint blockade in cancer therapy: The 2015 Lasker-DeBakey clinical medical research award. JAMA 314, 1113–1114 (2015). [PubMed: 26348357]
2. Sharma P, Allison JP, The future of immune checkpoint therapy. Science 348, 56–61 (2015). [PubMed: 25838373]
3. Topalian SL, Drake CG, Pardoll DM, Immune checkpoint blockade: a common denominator approach to cancer therapy. Cancer Cell 27, 450–461 (2015). [PubMed: 25858804]
4. Grosso JF, Jure-Kunkel MN, CTLA-4 blockade in tumor models: an overview of preclinical and translational research. Cancer Immun 13, 5 (2013). [PubMed: 23390376]
5. Hodi FS et al., Improved survival with ipilimumab in patients with metastatic melanoma. N Engl J Med 363, 711–723 (2010). [PubMed: 20525992]
6. Brahmer JR et al., Safety and activity of anti-PD-L1 antibody in patients with advanced cancer. N Engl J Med 366, 2455–2465 (2012). [PubMed: 22658128]
7. Alsaab HO et al., PD-1 and PD-L1 Checkpoint Signaling Inhibition for Cancer Immunotherapy: Mechanism, Combinations, and Clinical Outcome. Front Pharmacol 8, 561 (2017). [PubMed: 28878676]
8. Larkin J et al., Combined nivolumab and ipilimumab or monotherapy in untreated melanoma. N Engl J Med 2015, 23–34 (2015).

9. Boutros C et al., Safety profiles of anti-CTLA-4 and anti-PD-1 antibodies alone and in combination. Nat Rev Clin Oncol 13, 473–486 (2016). [PubMed: 27141885]
10. Postow MA, Sidlow R, Hellmann MD, Immune-Related Adverse Events Associated with Immune Checkpoint Blockade. N Engl J Med 378, 158–168 (2018). [PubMed: 29320654]
11. Boyman O, Sprent J, The role of interleukin-2 during homeostasis and activation of the immune system. Nature reviews. Immunology 12, 180–190 (2012).
12. Jiang T, Zhou C, Ren S, Role of IL-2 in cancer immunotherapy. Oncoimmunology 5, e1163462 (2016). [PubMed: 27471638]
13. Rosenberg SA et al., Treatment of 283 consecutive patients with metastatic melanoma or renal cell cancer using high-dose bolus interleukin 2. JAMA 271, 907–913 (1994). [PubMed: 8120958]
14. Rosenberg SA et al., Observations on the systemic administration of autologous lymphokine-activated killer cells and recombinant interleukin-2 to patients with metastatic cancer. N Engl J Med 313, 1485–1492 (1985). [PubMed: 3903508]
15. Klapper JA et al., High-dose interleukin-2 for the treatment of metastatic renal cell carcinoma : a retrospective analysis of response and survival in patients treated in the surgery branch at the National Cancer Institute between 1986 and 2006. Cancer 113, 293–301 (2008). [PubMed: 18457330]
16. Ishihara J et al., Matrix-binding checkpoint immunotherapies enhance antitumor efficacy and reduce adverse events. Sci Transl Med 9, eaan0401 (2017). [PubMed: 29118259]
17. Ricard-Blum S, The collagen family. Cold Spring Harb Perspect Biol 3, a004978 (2011). [PubMed: 21421911]
18. Dubois C, Panicot-Dubois L, Merrill-Skoloff G, Furie B, Furie BC, Glycoprotein VI-dependent and -independent pathways of thrombus formation in vivo. Blood 107, 3902–3906 (2006). [PubMed: 16455953]
19. Bergmeier W, Hynes RO, Extracellular matrix proteins in hemostasis and thrombosis. Cold Spring Harb Perspect Biol 4, a005132 (2012). [PubMed: 21937733]
20. Nagy J, Chang S, Dvorak A, Dvorak H, Why are tumour blood vessels abnormal and why is it important to know? Br J Cancer 100, 865 (2009). [PubMed: 19240721]
21. Liang H et al., A collagen-binding EGFR single-chain Fv antibody fragment for the targeted cancer therapy. J Control Release 209, 101–109 (2015). [PubMed: 25916496]
22. Liang H et al., A collagen-binding EGFR antibody fragment targeting tumors with a collagen-rich extracellular matrix. Sci Rep 6, 18205 (2016). [PubMed: 26883295]
23. Sabrkhany S, Griffioen AW, Oude Egbrink MG, The role of blood platelets in tumor angiogenesis. Biochim Biophysi Acta 1815, 189–196 (2011).
24. Zhou ZH et al., Reorganized collagen in the tumor microenvironment of gastric cancer and Its association with prognosis. J Cancer 8, 1466–1476 (2017). [PubMed: 28638462]
25. Provenzano PP et al., Collagen density promotes mammary tumor initiation and progression. BMC Med 6, 11 (2008). [PubMed: 18442412]
26. Shahidi M, Thrombosis and von Willebrand Factor. Adv Exp Med Biol 906, 285–306 (2017). [PubMed: 27628010]
27. Addi C, Murschel F, De Crescenzo G, Design and use of chimeric proteins containing a collagen-binding domain for wound healing and bone regeneration. Tissue Eng Part B Rev, 2, 163–182 (2016).
28. Ribba AS et al., Ser968Thr mutation within the A3 domain of von Willebrand factor (VWF) in two related patients leads to a defective binding of VWF to collagen. Thromb Haemost 86, 848–854 (2001). [PubMed: 11583318]
29. Ballmer-Weber BK, Dummer R, Küng E, Burg G, Ballmer PE, Interleukin 2-induced increase of vascular permeability without decrease of the intravascular albumin pool. Br J Cancer 71, 78–82 (1995). [PubMed: 7819054]
30. Mariathasan S et al., TGFβ attenuates tumour response to PD-L1 blockade by contributing to exclusion of T cells. Nature 554, 544–548 (2018). [PubMed: 29443960]

31. Zhu EF et al., Synergistic innate and adaptive immune response to combination immunotherapy with anti-tumor antigen antibodies and extended serum half-life IL-2. Cancer Cell 27, 489–501 (2015). [PubMed: 25873172]
32. Quezada SA, Peggs KS, Curran MA, Allison JP, CTLA4 blockade and GM-CSF combination immunotherapy alters the intratumor balance of effector and regulatory T cells. J Clin Invest 116, 1935–1945 (2006). [PubMed: 16778987]
33. Danhier F, Feron O, Preat V, To exploit the tumor microenvironment: Passive and active tumor targeting of nanocarriers for anti-cancer drug delivery. J Control Release 148, 135–146 (2010). [PubMed: 20797419]
34. Carnemolla B et al., Enhancement of the antitumor properties of interleukin-2 by its targeted delivery to the tumor blood vessel extracellular matrix. Blood 99, 1659–1665 (2002). [PubMed: 11861281]
35. Kufe DW, MUC1-C oncoprotein as a target in breast cancer: activation of signaling pathways and therapeutic approaches. Oncogene 32, 1073–1081 (2013). [PubMed: 22580612]
36. Mach J-P et al., Use of radiolabelled monoclonal anti-CEA antibodies for the detection of human carcinomas by external photoscanning and tomoscintigraphy. Immunol Today 2, 239–249 (1981). [PubMed: 25290651]
37. Busek P, Mateu R, Zubal M, Kotackova L, Sedo A, Targeting fibroblast activation protein in cancer - Prospects and caveats. Front Biosci (Landmark edition) 23, 1933–1968 (2018).
38. Maeda H, Wu J, Sawa T, Matsumura Y, Hori K, Tumor vascular permeability and the EPR effect in macromolecular therapeutics: a review. J Control Release 65, 271–284 (2000). [PubMed: 10699287]
39. Swartz MA, Fleury ME, Interstitial flow and its effects in soft tissues. Annu Rev Biomed Eng 9, 229–256 (2007). [PubMed: 17459001]
40. Lim SY et al., Circulating cytokines predict immune-related toxicity in melanoma patients receiving anti-PD-1-based immunotherapy. Clin Cancer Res, Epub ahead of print (2018).
41. Pillai RN et al., Comparison of the toxicity profile of PD-1 versus PD-L1 inhibitors in non-small cell lung cancer: A systematic analysis of the literature. Cancer 124, 271–277 (2018). [PubMed: 28960263]
42. Simpson TR et al., Fc-dependent depletion of tumor-infiltrating regulatory T cells co-defines the efficacy of anti-CTLA-4 therapy against melanoma. J Exp Med 210, 1695–1710 (2013). [PubMed: 23897981]
43. Hadrup S, Donia M, Thor Straten P, Effector CD4 and CD8 T cells and their role in the tumor microenvironment. Cancer Microenviron 6, 123–133 (2013). [PubMed: 23242673]
44. Bethune MT, Joglekar AV, Personalized T cell-mediated cancer immunotherapy: progress and challenges. Curr Opin Biotechnol 48, 142–152 (2017). [PubMed: 28494274]
45. Lambert JM, Chari RV, Ado-trastuzumab Emtansine (T-DM1): an antibody-drug conjugate (ADC) for HER2-positive breast cancer. J Med Chem 57, 6949–6964 (2014). [PubMed: 24967516]
46. Ishihara J et al., Improving Efficacy and Safety of Agonistic Anti-CD40 Antibody Through Extracellular Matrix Affinity. Mol Cancer Ther 17, 2399–2411 (2018). [PubMed: 30097487]
47. Lee SS, Bindokas VP, Kron SJ, Multiplex three-dimensional optical mapping of tumor immune microenvironment. Sci Rep 7, 17031 (2017). [PubMed: 29208908]

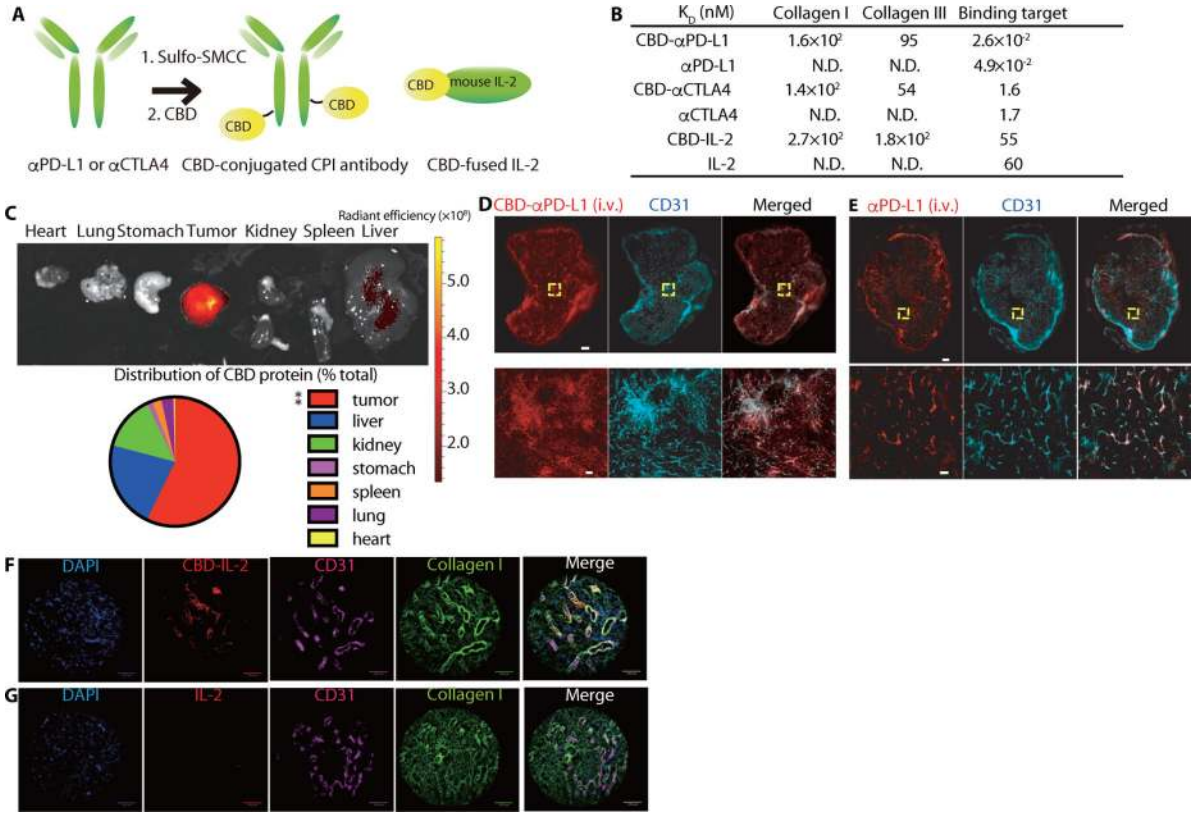


**Fig. 1. CBD protein localizes to tumors after i.v. injection through collagen affinity.**

(A) Schematic of conjugation of a collagen-binding domain (CBD), the recombinant VWF A3 domain, to checkpoint inhibitor (CPI) antibody, resulting in affinity for collagen. CBD-fused IL-2 was recombinantly expressed, with the CBD on the N-terminus of IL-2 using a $(GGGS)_2$ linker. (B) Dissociation constants ($K_D$ values) of CBD- and unmodified aPD-L1, αCTLA4, and IL-2 against collagen type I and collagen type III, recombinant mouse (rm)CTLA4, rmPD-L1, and/or rmIL-2Ra were measured by ELISA. N.D.= not determined because of low signals. Graphs of concentrations vs signals are shown in fig. S2. (C) $5 \times 10^5$ MMTV-PyMT cells were inoculated in the mammary fat pad. When the tumor volume reached 500 $mm^3$, 300 μg of DyLight 800-labeled CBD was injected i.v.. A pie chart represents the biodistribution of CBD protein 48 hr after injection as determined by fluorescence analysis of each organ (n = 4). (D) Intratumoral imaging was performed on MMTV-PyMT tumors when they reached 200 $mm^3$ by injecting 100 μg of DyLight 594-labeled CBD-αPD-L1 or (E) 100 μg of DyLight 594-labeled αPD-L1 i.v. 30 min after injection. The tumor was then harvested, and fluorescence was analyzed by microscopy. Top panels: images of whole tumors, scale bar = 500 μm. Bottom panels: images of enlarged yellow squares within upper panels, scale bar = 50 μm. Representative images of 2 tumors each. (F, G) Binding of (F) CBD-IL-2 or (G) unmodified IL-2 to human melanoma cryosections was imaged by fluorescence microscopy. Scale bar = 100 μm. Two experimental replicates. Statistical analyses were done using ANOVA with Tukey's test. $^{**}p < 0.01$.

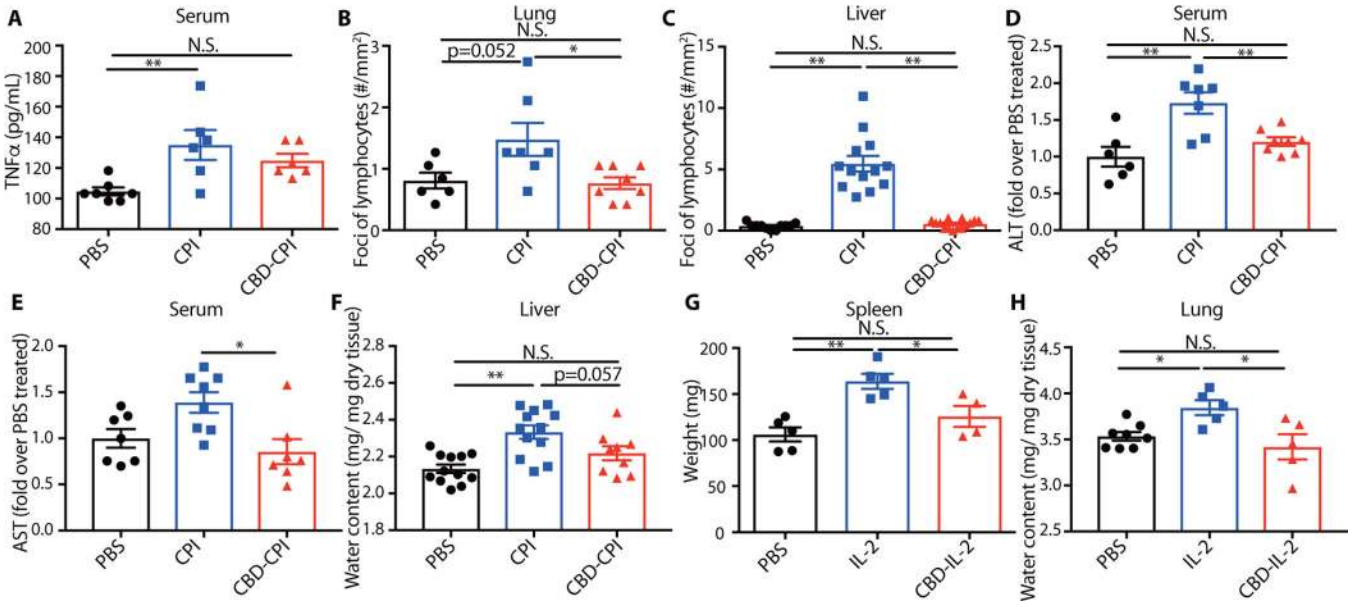


**Fig. 2. CBD fusion reduces treatment-related toxicity of immunotherapeutic drugs.**

Adverse events were studied in mice bearing B16F10 melanomas. $5 \times 10^5$ B16F10 cells were inoculated on day 0. (A-F) CBD- or unmodified αCTLA4 and αPD-L1 (100 μg each/injection) were injected i.v. on day 4 and 7. (A) On day 8, serum concentrations of TNFα in blood plasma were measured (mean ± SEM). (B, C) On day 10, the numbers of lymphocytic infiltration spots in histologic (B) lung and (C) liver sections were counted and divided by area (mean ± SEM). (D, E) On day 10, blood serum (D) ALT and (E) AST activities were measured (mean ± SEM). (F) On day 10, the liver was harvested and weighed. Water content in the liver was determined by weighing before and after lyophilization and was normalized to dry tissue weight (mean ± SEM). (G, H) $5 \times 10^5$ B16F10 cells were inoculated on day 0. CBD-IL-2 (6 μg for IL-2 basis) or unmodified IL-2 (6 μg) was injected i.v. on day 7, 8, and 9. On day 10, (G) spleen and (H) lung were harvested and weighed. Water content in the lung was determined as described above (mean ± SEM). Statistical analyses were done using ANOVA with Tukey's test. Kruskal-Wallis test followed by Dunn's multiple comparison was used in (C) due to nonparametric data. Two experimental replicates. $*p < 0.05$; $**p < 0.01$; N.S. = not significant.

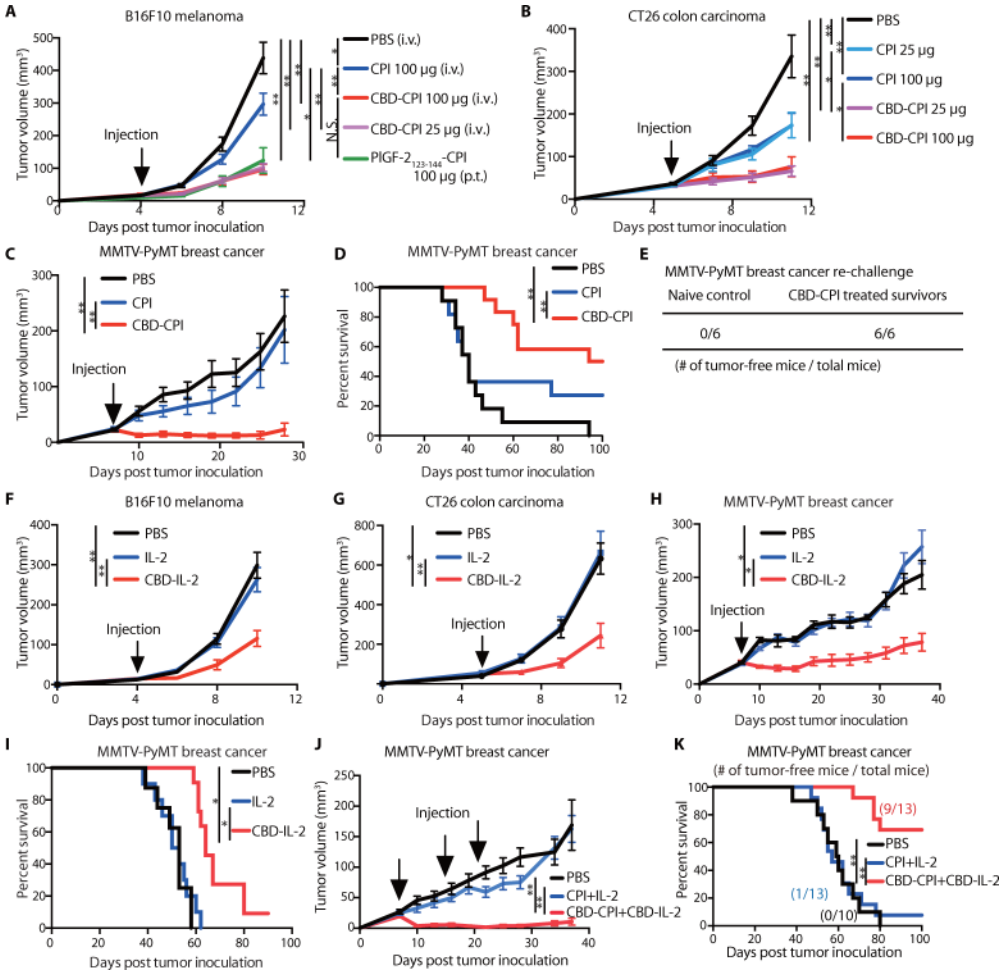


**Fig. 3. Both CBD-CPI and CBD-IL-2 treatments reduce tumor growth in 3 murine tumor models.**

We used three tumor models to study efficacy of targeted immunotherapy, namely the B16F10 melanoma model, the CT26 colon carcinoma model, and the MMTV-PyMT breast cancer model. (A, F) $5 \times 10^5$ B16F10 cells were inoculated on back skin, (B, G) $5 \times 10^5$ CT26 cells were inoculated on back skin, (C, D, H-K) $5 \times 10^5$ MMTV-PyMT cells were inoculated on the right mammary fat pad day 0. (A-D) CBD-αCTLA4 + CBD-PD-L1 (CBD-CPI), αCTLA4 + αPD-L1 (CPI) or PBS was administered on (A) day 4, (B) day 5, (C, D) day 7. (A) CBD- and unmodified CPI were injected i.v., and PlGF-$2_{123–144}$-CPI was injected peritumorally (p.t.). Antibody doses per administration are indicated on the figure. (A-C) Graphs depict tumor volume until the first mouse died and (D) survival rate. (E) 30 days after the first tumor inoculation in the right mammary gland fat pad, $5 \times 10^5$ MMTV-PyMT cells were again inoculated into the left mammary gland fat pad in CBD-CPI treated tumor-free survivors or in naïve mice. Numbers indicate how many mice remain tumor-free among total mice after 40 days of tumor re-challenge. (F) $5 \times 10^5$ B16F10 cells were inoculated on the back skin, (G) $5 \times 10^5$ CT26 cells were inoculated on the back skin, (H-K) $5 \times 10^5$ MMTV-PyMT cells were inoculated on the right mammary fat pad day 0. (F-I) 6 μg IL-2 or equimolar CBD-IL-2 was injected i.v. on (F) day 4, (G) day 5, (H, I) day 7. (F-H) Graphs depict tumor volume until the first mouse died and (I) survival rate. (J, K) After 7,

14, and 21 days from tumor inoculation, CBD-αCTLA4 + CBD-αPD-L1 (CBD-CPI) + CBD-IL-2, αCTLA4 + αPD-L1 (CPI) + IL-2 or PBS were injected i.v.. (J) Graphs depict tumor volume until the first mouse died and (K) survival rate. Numbers indicate how many mice remained tumor-free among total mice 100 days after tumor inoculation. (A) PBS, n = 9; CPI 100 μg and CBD-CPI 25 μg, n = 8; CBD-CPI 100 μg and PlGF-$2_{123–144}$-CPI 100 μg, n = 7. (B) PBS and CPI 25 μg, n = 11; CPI 100 μg and CBD-CPI 25 μg, n = 10; CBD-CPI 100 μg, n = 9. (C, D) CBD-CPI, n = 12; other groups, n = 11. (E-G) n = 6. (H, I) PBS, n = 10; other groups, n = 11. (J, K) PBS, n = 10; other groups, n = 13. Tumor volumes are presented as mean ± SEM. Two experimental replicates. Statistical analyses were done using ANOVA with Tukey's test for tumor size and Log-rank (Mantel-Cox) test for survival curves. *$p < 0.05$; **$p < 0.01$.

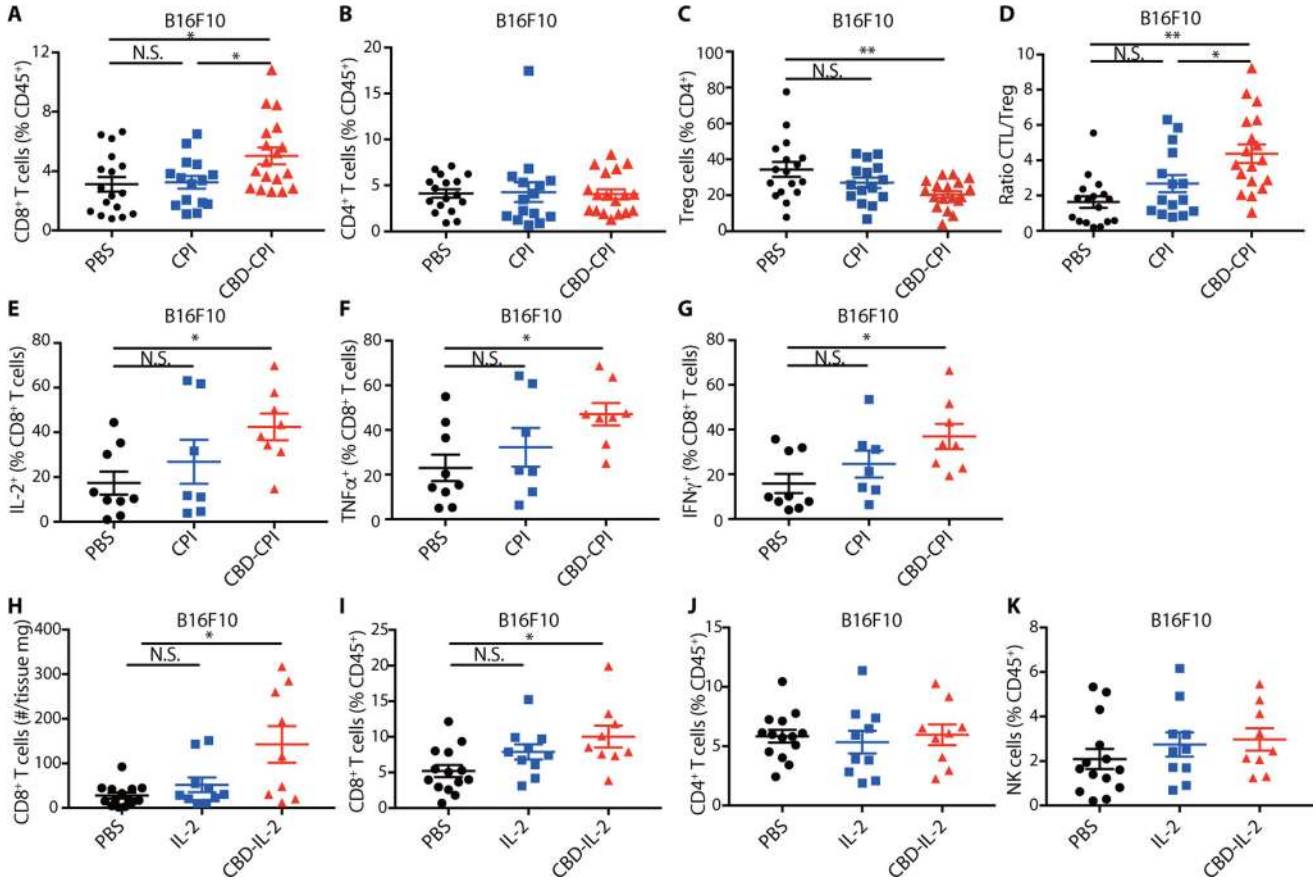


**Fig. 4. Both CBD-CPI and CBD-IL-2 treatments increase B16F10 melanoma-infiltrating cytotoxic CD8$^+$ T cells.**

We used the B16F10 model to study T cell behavior in tumors with targeted immunotherapy. $5 \times 10^5$ B16F10 cells were inoculated on day 0. CBD-αCTLA4 + CBD-αPD-L1 (CBD-CPI), αCTLA4 + αPD-L1 (CPI), or PBS was administered on day 4. CPI was injected i.v. at 100 μg each. Tumors were collected on day 8, followed by flow cytometric analysis. Frequency of (A) CD8$^+$CD3$^+$ and (B) CD4$^+$CD3$^+$ tumor-infiltrating T cells within CD45$^+$ lymphocytes and (C) Treg (Foxp3$^+$CD25$^+$) of CD4$^+$CD3$^+$ tumor-infiltrating T cells. (D) The ratio of cytotoxic T lymphocytes (CTL; CD62L$^-$CD44$^+$CD8$^+$CD3$^+$) versus Treg (Foxp3$^+$CD25$^+$CD4$^+$). (E-G) T cells were extracted from the tumors and stimulated with aCD28 and aCD3 for 6 hours. Graphs depict the % of (E) IL-2$^+$, (F) TNFα$^+$, (G) IFNγ$^+$ of CD8$^+$CD3$^+$ T cells. (H-K) CBD-IL-2, IL-2, or PBS was administered on day 7, 8 and 9. Lymphocytes were extracted from the tumor on day 10, followed by flow cytometric analysis. Graphs depict the number of (H) CD8$^+$CD3$^+$ T cells per tumor weight (mg), the frequency of (I) CD8$^+$CD3$^+$ T cells within total CD45$^+$ lymphocytes, (J) CD4$^+$CD3$^+$ T cells within total CD45$^+$ lymphocytes, and (K) NK1.1$^+$CD3$^-$ NK cells within total CD45$^+$ lymphocytes. Lines represent mean ± SEM. Two experimental replicates. Statistical analyses were done using ANOVA with Tukey's test. Kruskal-Wallis test followed by Dunn's multiple comparison was used in (H) due to nonparametric data. *$p < 0.05$; **$p < 0.01$.